Improving mechanical properties and sustainability of high-strength engineered cementitious composites (ECC) using diatomite

Zhu, Xuezhen; Zhang, Minghu; Shi, Jinyan; Weng, Yiwei; Yalçınkaya, Çağlar; Šavija, Branko

DOI
10.1617/s11527-023-02283-w

Publication date
2024

Document Version
Final published version

Published in
Materials and Structures/Materiaux et Constructions

Mater Struct (2024) 57:11
https://doi.org/10.1617/s11527-023-02283-w

ORIGINAL ARTICLE

Improving mechanical properties and sustainability of high-strength engineered cementitious composites (ECC) using diatomite

Xuezhen Zhu · Minghu Zhang · Jinyan Shi · Yiwei Weng · Çağlar Yalçınkaya · Branko Šavija

Received: 20 April 2023 / Accepted: 11 December 2023

Abstract High-strength engineered cementitious composites (ECC) typically require higher cement content, which is negative from the sustainability point of view. To alleviate this problem, herein a low-cost and eco-friendly high-strength ECC (with a compressive strength of over 100 MPa) was developed, and diatomite was used to replace a small amount of cement. An appropriate amount of diatomite was found to improve the compressive strength, tensile strength and first cracking strength of ECC, but at the expense of part of the strain capacity (still all higher than 2.9%). Furthermore, the high pozzolanic activity and specific surface area of diatomite also increased the autogenous shrinkage, but reduced the drying shrinkage of ECC due to its internal curing effect. The incorporation of diatomite improved the pore structure of ECC, consumed more $Ca(OH)_2$, and enhanced the hydration degree of the mixture. In the end, the economic and environmental benefits of diatomite-modified ECC were also evaluated, and the cost, non-renewable energy demand, and global warming potential of ECC with 3% diatomite were reduced compared to plain ECC by 12.9, 15.1, and 13.3%, respectively. The developed high-strength ECC is therefore a low-cost and eco-friendly alternative to the traditional one.

Keywords Diatomite · High-strength · Engineered cementitious composites (ECC) · Tensile properties · Sustainability assessment

1 Introduction

In recent decades, super high-rise buildings, submarine tunnels, dams, and protection projects have been constructed, increasing the requirements for cement-based materials, including high strength, high ductility, and excellent durability [1, 2]. However, compressive strength and ductility are contradictory requirements for cement-based materials, as high-strength concrete tends to be more brittle [3]. Therefore, low ductility and propensity to cracking are some of the key factors hindering the long-term

Supplementary Information The online version contains supplementary material available at https://doi.org/10.1617/s11527-023-02283-w.

X. Zhu · M. Zhang · J. Shi (✉)
School of Civil Engineering, Central South University, Changsha 410075, People's Republic of China
e-mail: jinyan.shi@csu.edu.cn

Y. Weng
Department of Building and Real Estate, The Hong Kong Polytechnic University, Hong Kong, China

Ç. Yalçınkaya
Department of Civil Engineering, Faculty of Engineering, Dokuz Eylül University, İzmir, Türkiye

B. Šavija
Faculty of Civil Engineering and Geosciences, Delft University of Technology, Delft, The Netherlands

Published online: 02 January 2024

service of high-strength concrete. Although steel reinforcement is normally used to improve the ductility of reinforced concrete (RC) structures, the concrete cover remains at risk from cracking, which may seriously affect the long-term service life of RC structures, especially in aggressive environments [4, 5].

To address the issue of low ductility in cementitious materials, engineered cementitious composites (ECC) have been developed. ECCs have high ductility under tensile conditions. ECC typically contains a large amount of fibers and no coarse aggregates, allowing it to achieve high strain capacity (2−8%), hundreds of times that of ordinary concrete [6]. Furthermore, ECCs can have a high compressive strength, and recent studies have shown a compressive strength of 85−167 MPa can be achieved while guaranteeing a tensile strain capacity of 1.2−6.5% [7, 8]. ECC exhibits stress-hardening and multiple-cracking behavior under uniaxial tension, which is different from the localized cracking occurring in classical or fiber-reinforced concrete. Furthermore, ECC is characterized by small cracks (usually below 100 μm wide) after tensile loading. Such cracks typically have less effect on concrete durability, and allow for a good self-healing capacity [9]. Therefore, high-strength and high-ductility ECCs may be a suitable alternative for existing cement-based materials, especially for structural reinforcement.

As one of the major contributors to man-made CO_2, the cement industry produces about 8% of global CO_2 emissions [10]. A ton of Portland cement (PC) produced contributes 0.87 ton of CO_2. In ECCs, the cement content can reach 1126 kg/m^3 due to the lack of coarse aggregate [11]. To reduce the environmental load of ECC, replacing part of the cement with supplementary cementitious materials (SCMs, e.g. fly ash (FA), ground granulated blast slag (GGBS), and silica fume (SF)) is a common strategy. SCM is the indispensable components of ECC, and its incorporation can reduce matrix fracture toughness or improve the fiber dispersion degree, thereby achieving the excellent harden-straining performance of ECC. FA is the most common SCM in ECC, and its content can reach 1.0−2.3 times that of cement in ECC [12]. Wu et al. used 31.3% cement and 68.7% FA to prepare ECC, and its 28-day compressive strength can reach 41.9 MPa, which can be used in ordinary buildings [13]. For high-strength ECC (HS-ECC), cement: FA: SF of 1:0.8:0.18 is a common mix proportion, and its 28-day compressive strength can reach more than 80 MPa [14]. On this basis, further reducing the cement content and material cost while improving its compressive strength is the key to promoting its application in large-scale projects.

Diatomite is a porous siliceous soil, and has low density, high porosity, and high adsorption capacity. The world's diatomite reserves are abundant (at least 2 billion tons), and they are mainly distributed in China, Denmark, the United States, and France [15]. Diatomite is rich in SiO_2 (86−94 wt%) [16] and has a small amount of clay minerals and organic matter. Furthermore, the porosity of diatomite is relatively high, which can reach 80−90% [17]. In low-quality diatomite, which is mixed with calcite, clay minerals, and organic matter, the SiO_2 content is as low as 50%. However, even when the cost and the carbon emissions required to purify diatomite are considered, they are far lower than those associated with production of PC [18–20]. Diatomite is a highly active SCM, and replacing PC with it may produce a similar effect to SF [21, 22]. In addition, diatomite is an economical SCM, and its average cost is only 10 USD/ton which is higher than that of SF (1000 USD/ton). In the United States, the cost of diatomite is only 9/100 of that of a PC [20, 23]. Besides, with the implementation of sustainable development policies, the supply of traditional SCMs have gradually become insufficient. Therefore, using a small amount of diatomite instead of PC to produce an ECC mixture is practically attractive. However, diatomite has not been extensively studied as a SCM, especially with respect to application in ECCs.

Although some studies have investigated the properties of traditional cement-based materials containing diatomite, the influence mechanism of diatomite on the matrix fracture toughness and cohesion force of fiber/matrix interface is lack, which makes the evolution mechanism of cracking behavior for the ECC under tensile loading is not clear. Therefore, a small amount of diatomite was used to replace the PC to avoid an excessive decrease in the ductility of HS-ECC, and its mechanical properties and volume stability were investigated. Meanwhile, various microstructure tests were carried to comprehensively explain the evolution of macroscopic properties of HS-ECC. In addition, the cost, carbon emissions, and global warming potential of diatomite-modified HS-ECC were discussed. This study provides a new

effective way to solve the insufficient strength of HS-ECC components and improves the utilization value of diatomite in the construction industry.

2 Experimental program

2.1 Materials

HS-ECC consists of cement, FA, SF, silica sand, fiber, diatomite, superplasticizer, and water as raw materials. Ordinary PC (P·O 42.5), class I FA and SF are adopted as binder. Due to its pozzolanic activity and filling effect, SF was adopted to increase the mechanical strength and toughness of HS-ECC. The diatomite was used to produce HS-ECC, and its water absorption is 1.0 g/g [24]. The chemical compositions of cementitious materials were analyzed through the X-ray Fluorescence (XRF), and their results are listed in Table 1. Silica sand with a particle size of 120−180 μm was utilized as fine aggregate to enhance the packing density. Fig. S1 plots the particle size distributions of the raw materials. The length and diameter of the polyethylene (PE) fiber were 18 mm and 15.6 μm, respectively. The elastic modulus and density of the PE fiber were 147 GPa and 0.97 g/cm^3, respectively. The polycarboxylate-based superplasticizer (SP), purchased from Shanxi Qinfen Building Materials Co., Ltd, was used to maintain the fluidity of the HS-ECC mixture.

2.2 Mix proportion

The diatomite was used to replace the same weight of cement, and its contents were 1, 3, and 5% (See Table 2). The mixture was denoted as DX, where the letters "D" and "X" represent diatomite and the substitution level of diatomite, respectively. HS-ECC without diatomite was regarded as the control mixture (D0). The water/binder ratio of the mixture was 0.2, and the volume content of fiber was 2%, which is a common mix proportion [14].

2.3 Specimen preparation

Preparation process of HS-ECC is shown in Fig. S2. Before the experiment, diatomite absorbed water under vacuum for 2 h. During the mixing process, the cement, FA, SF, diatomite, and sand were first mixed for 2 min at low speed. The water and SP were then added and mixing continued for 4 min at low speed. After the addition of fiber, the mixture was mixed for 4 min at low speed and then for 6 min at high speed to ensure good fiber dispersion. The mixture was poured into the mold and covered with plastic film to prevent the water evaporation. The specimens were cured at 20 °C for 24 h and then demolded. After demolding, the samples were cured at a temperature of 20 ± 2 °C and relative humidity of 95% until the specific ages.

Table 1 Chemical composition of cementitious material (wt.%)

Type	SiO_2	Al_2O_3	CaO	MgO	Fe_2O_3	SO_3	K_2O	TiO_2	Na_2O	P_2O_5	Cr_2O_3	LOI
Diatomite	93.22	2.75	0.35	0.23	1.96	0.43	0.55	0.27	0.19	0.05	0.02	7.61
FA	52.4	35.3	2.61	0.73	2.81	0.47	1.42	1.61	0.67	–	–	2.86
Cement	21.18	7.16	62.1	2.01	3.50	2.56	–	–	–	–	–	2.40
SF	91.60	0.36	1.13	0.60	0.08	–	–	–	–	–	–	2.48

Table 2 Mix proportion of HS-ECC (kg/m^3)

Mixture	Cement	Diatomite	FA	SF	Sand	Water	SP	Fiber (Vol.%)
D0	750.0	0.0	600	135	450	300	7.35	2
D1	742.5	7.5	600	135	450	300	8.17	2
D3	727.5	22.5	600	135	450	300	8.79	2
D5	712.5	37.5	600	135	450	300	9.90	2

2.4 Test methods

2.4.1 Compressive strength

According to the standard GB/T 17671-1999 [25], cubic specimens (40 × 40 × 40 mm) were prepared to measure the compressive strength of HS-ECC at ages of 3, 7, and 28 days using a WAW-600 servo-hydraulic testing machine. The loading rate was 2.4 kN/s, and six specimens of each mixture were tested at each age.

2.4.2 Three-point bending

The three-point bending test was performed to evaluate the fracture toughness and the elastic modulus of the HS-ECC matrix according to ASTM E399 [26, 27], which were calculated by Eqs. (1−5). The prismatic specimens with the size of 40 × 40 × 160 mm were utilized in this experiment, and the ratio of the notch depth to the height of the specimen at the mid-span position was 0.4. Fig. S3 shows the schematic diagram of the three-point bending test, and the loading rate was 0.5 mm/min.

$$E_m = 0.83 \times 2.15 \times 10^4 \times \sqrt[3]{\frac{\sigma_m}{10}} \tag{1}$$

$$K_m = \frac{3f_{(\alpha)}(P_c + 0.5W_h)\sqrt{a_0}}{2h^2 t} S \tag{2}$$

$$W_h = \frac{W_{h_0} S}{L} \tag{3}$$

$$f_{(\alpha)} = \frac{1.99 - \alpha(1-\alpha)(2.15 - 3.93\alpha + 2.7\alpha^2)}{(1+2\alpha)\sqrt{(1-\alpha)^3}} \tag{4}$$

$$\alpha = \frac{a_0}{h} \tag{5}$$

where, E_m represents the elastic modulus of the matrix, GPa; σ_m represents the compressive strength of the matrix, MPa; K_m represents the fracture toughness of the matrix, MPa·m$^{1/2}$; P_c represents the peak load, kN; W_{h_0} represents the self-weight of the specimen, kN; S represents the beam span, mm; L, h, t represent the length, thickness, and width of the specimen, respectively, mm; a_0 represents the depth of the notch in the specimen, mm.

2.4.3 Uniaxial tensile

Dumbbell-shaped specimens were adopted to measure the tensile properties of HS-ECC according to JSCE [28]. The length, width, and height of the dumbbell-shaped specimen were 320, 60, and 13 mm, respectively. The loading rate of the specimen was 0.5 mm/min in the experiment. The length change at the middle position of the HS-ECC specimen is measured by two external linear variable displacement transducers (LVDTs). Fig. S4 shows the schematic diagram of the uniaxial tensile test. Eventually, the strain value of HS-ECC was calculated from the average measurement value of LVDTs. Besides, the average crack width of HS-ECC was defined by the ratio of the tensile elongation length to the crack number in the test location (80 mm) of the dumbbell-shaped specimen without loading.

2.4.4 Volume stability

The corrugated tube method was used to measure the autogenous shrinkage of HS-ECC mixture according to ASTM C 1698-09. The length and diameter of the corrugated tube were 420 and 30 mm, respectively. When the specimen reached final setting, data acquisition system begined to collect the autogenous shrinkage value and lasted for 14 days. The measurement device of the autogenous shrinkage test is drawn in Fig. S5a.

Three prismatic specimens with a size of 25 × 25 × 280 mm were used to measure the drying shrinkage of HS-ECC samples. The drying shrinkage of the specimens was measured at various ages until 56 d, according to the ASTM C596-01 [29]. During the test, the environmental temperature and relative humidity of drying shrinkage were 23 ± 2 °C and 60%, respectively. The measuring instrument is schematically shown in Fig. S5(b).

2.4.5 Microstructure

The crystal phase of the HS-ECC paste at the age of 28 d was analyzed by the X-ray diffraction (XRD) test. During the sample preparation process, samples were soaked in isopropanol for 7 d to terminate

hydration. After drying under vacuum conditions for 7 d, the sample was ground into powder (below 75 μm). This XRD test was performed with an X'Pert PRO MPD, and the determination angle (2θ) range is 5°−60° with a speed of 10°/min. The derivative thermogravimetric (DTG) test was performed to characterize the content of hydration products of HS-ECC paste. About 100 mg of sample was prepared, following the same procedure as that for the XRD test. In DTG, the sample was heated from 30 to 1000 °C under the N_2 condition with a heating rate of 10 °C/min.

To further reveal the influence mechanism of diatomite content on the reaction degree of HS-ECC paste, the non-evaporable water content (NEWC) of paste was evaluated according to the DTG test, as shown in Eq. (6). Besides, the $Ca(OH)_2$ (CH) content of paste was evaluated by Eq. (7).

$$W_{\mathrm{NEWC}} = \left[\frac{M_{105} - M_{950}}{M_{105}} - \left(f_C \times LOI_C + f_{FA} \times LOI_{FA} + f_{SF} \times LOI_{SF} + f_D \times LOI_D\right)\right] \times 100\% \tag{6}$$

$$W_{CH} = \left(\frac{M_{410} - M_{500}}{M_{Total}} \times \frac{74}{18} + \frac{M_{500} - M_{780}}{M_{Total}} \times \frac{74}{44}\right) \times 100 \tag{7}$$

where, W_{NEWC} and W_{CH} represent the NEWC and CH content, %; M_{105}, M_{410}, M_{500}, M_{780} and M_{950} represent the mass of the sample at 105, 410, 500, 780, and 950 °C, respectively, μg. M_{Total} represents the unheated mass of the sample, μg. LOI_C, LOI_{FA}, LOI_{SF}, and LOI_D represent the loss on ignition of cement, FA, SF, and diatomite, respectively. f_C, f_{FA}, f_{SF}, and f_D represent the mass fraction of cement, FA, SF, and diatomite in the cementitious material, respectively.

The bonding mechanism of hydration products of HS-ECC paste was measured according to the Fourier Transform Infra-Red (FT-IR) spectra, and the wave test range was between 500 and 4000 cm^{-1}. The specimens were prepared following the same procedure as for the XRD test. Mercury Intrusion Porosimetery (MIP) was used to analyze the pore structure of HS-ECC paste with diatomite. Samples were cut into small pieces with a size of 5−7 mm and then soaked in isopropanol. Before the experiment, the sample was dried in the vacuum dryer for 7 d. A scanning electron microscope (SEM) test (TESCAN MIRA 4) was used to study the morphology of fiber in HS-ECC at 28 d after the tensile experiment. Samples were collected from the fracture site of specimen after tensile loading, and their were coated with gold before the SEM analyses.

2.4.6 Environmental impact and economic benefits

Reducing the cost and environmental load of HS-ECC is a strategy to advance its engineering application. Based on the types of substances emitted by raw materials, the global warming potential (CO_2-eq, GWP), non-renewable cumulative energy demand (nr-CED), photochemical ozone creation potential (C_2H_4-eq, POCP), ozone depletion potential (CFC11-eq, ODP), nutrification potential (PO_4-eq, NP), and acidification potential (SO_2-eq, AP) parameters of the HS-ECC mixture were used to evaluate its environmental benefits, and the cost was also used to evaluate its economic benefits [30, 31]. The standardized eco-balance method correspond to the European standards EN ISO 14040 and EN ISO 14044. These parameters were obtained from other literature, as shown in Table S1.

3 Results and discussion

3.1 Compressive strength

Compressive strength of HS-ECC with different diatomite contents is shown in Fig. 1. The 28-day compressive strength of all samples is 86.0−101.7 MPa, all within the strength range of HS-ECC (> 80 MPa) [7]. Compared with the control specimen (D0), the 28-d compressive strength of D1, D3, and D5 approximately increased by 6.9, 18.3, and 10.2%, respectively. At the same age, the strength of HS-ECC first increased and then decreased with the increase of diatomite content. At 28 days, the compressive strength of HS-ECC containing 3% diatomite reached the maximum value. The diatomite particles improve the compressive strength HS-ECC through the filling effect and the pozzolanic effect [31, 32]. The particle

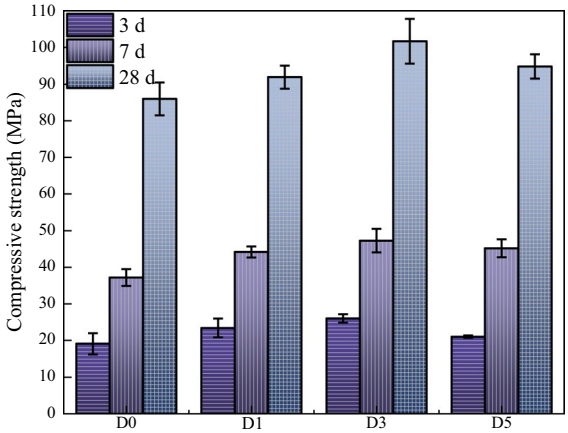

Fig. 1 Compressive strength of HS-ECC with various diatomite contents

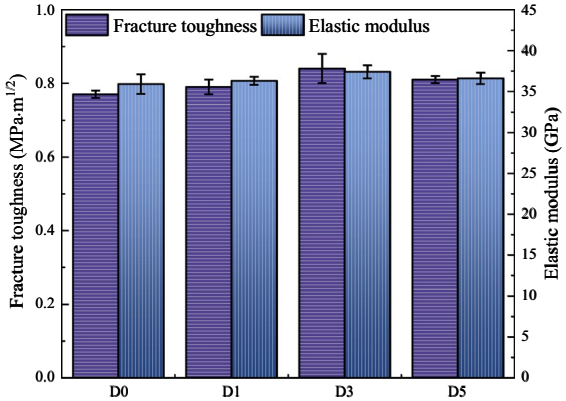

Fig. 2 The influence of diatomite content on the fracture toughness and elastic modulus of HS-ECC at 28 days

size of diatomite is significantly smaller than that of cement and SF (See Fig. S1). Fine diatomite particles effectively fill the internal pores of the HS-ECC matrix, thereby improving the pore structure of specimen. Meanwhile, amorphous SiO_2 from diatomite dissolves and then reacts with CH during the curing process, increasing the hydration degree of HS-ECC system [33]. Moreover, diatomite has an internal curing effect, which promotes the hydration of cement particles and the pozzolanic reaction of FA/SF particles. When the diatomite content was within 3%, the compressive strength of HS-ECC containing diatomite increased with increasing the diatomite content. In this study, the diatomite replaced the cement with the same weight, thereby diluting the cement system. When the diatomite content was 5%, the negative effect of dilution on the compressive strength of HS-ECC is more pronounced than the positive effects described above. Consequently, at the same curing ages (3, 7 and 28 d), the compressive strength of D5 was lower than that of the D3 specimen. However, the compressive strength of HS-ECC containing 5% diatomite at the same age was still higher than that of the control sample (D0), which indicates that the incorporation of diatomite promotes the compressive strength development of the HS-ECC system.

3.2 Fracture toughness and elastic modulus

Figure 2 shows the fracture toughness of the HS-ECC matrix with diatomite [34]. The fracture toughness of HS-ECC matrix first increases and then decreases with the increase of diatomite content. The increase in fracture toughness is detrimental to the multiple cracking capacity of ECC since the generation of new cracks requires more energy [35]. This therefore results in a reduction in the number of cracks under tensile load. The effect of diatomite content on the elastic modulus of the HS-ECC matrix at 28 days is also shown in Fig. 2. The elastic modulus of the D1, D3, and D5 specimens increased to 36.3, 37.4, and 36.6 GPa, respectively, compared to the D0 sample (35.9 GPa). With the increase in diatomite content, the elastic modulus of the HS-ECC matrix first increases and then decreases. Combined with the results of compressive strength, it was found that the elastic modulus of the HS-ECC matrix increased gradually with the increase of compressive strength, which is consistent with the conclusion of Zhang et al. [14].

3.3 Tensile properties

The uniaxial tensile stress–strain curves of HS-ECC with different diatomite contents are show in Fig. 3. All HS-ECC specimens exhibited multiple cracking characteristics and significant strain-hardening behavior. Their strain capacity ranged from 2.9 to 3.9%. The tensile parameters of HS-ECC with different diatomite contents are plotted in Fig. 4. Compared with first cracking strength of D0 (5.82 MPa), the first cracking strength of D1, D3, and D5 were 6.07, 6.90, and 6.55 MPa, which is an increase of 4.3, 18.6,

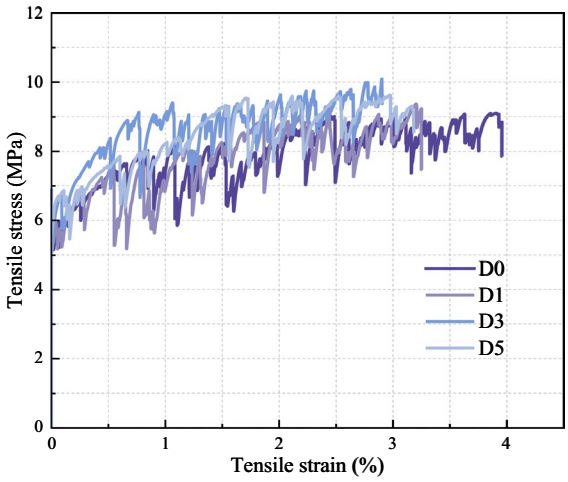

Fig. 3 Tensile stress–strain curves of HS-ECC with various diatomite contents

and 12.5%, respectively. The first cracking strength of HS-ECC presents a trend to increase first and then decrease due to the incorporation of diatomite, which is usually positively correlated with the fracture toughness of the ECC matrix [14]. When the content of diatomite was 3%, the first cracking strength of HS-ECC reached the maximum value. In summary, the incorporation of diatomite can delay the occurrence of cracks in ECC under loading, which is beneficial in practical engineering applications. With the increase of the diatomite content, the fracture toughness of the matrix first increases and then decreases, so the first cracking strength also shows the same development trend. It should be noted, however, that high first-cracking strength is usually detrimental to the multiple-cracking behavior of ECC.

Compared with the ultimate tensile strength of the control specimen of D0 (9.11 MPa), the ultimate tensile strength of D1, D3, and D5 specimens increased to 9.37, 10.09, and 9.63 MPa, which is an increase of 2.9, 10.8, and 5.7%, respectively (See Fig. 4b). The ultimate tensile strength of HS-ECC first increased and then decreased with the increase in diatomite replacement ratio. Among all specimens, the D3 specimen had the highest ultimate tensile strength. This may be due to the pozzolanic reaction and filling effect of diatomite. The pozzolanic reaction and filling effect of diatomite improved the cohesion force of the fiber/matrix interface. However, at higher replacement levels, the excess diatomite may significantly dilute the cement system and thus reducing the content of hydration products in paste, which was detrimental to the development of the cohesion force of the fiber/matrix interface. Therefore, the ultimate tensile strength of D5 was lower than that of the D3 sample.

Compared with the strain capacity of the reference mixture of D0 (3.9%), the strain capacities of D1, D3, and D5 decreased to 3.2, 2.9, and 2.96%, respectively (See Fig. 4). The strain capacity of HS-ECC first decreased and then increased slightly with increasing the diatomite content. This may be related to the fracture toughness of the HS-ECC matrix. Incorporating a small amount of diatomite increased the fracture toughness of the HS-ECC matrix, which reduced the probability to generate many cracks in HS-ECC. Among all specimens, the D3 sample showed the lowest strain capacity, however it was still about 300 times that of ordinary concrete [36]. This indicates that the D3 sample still has an excellent strain hardening behavior.

The number of cracks and average crack width of HS-ECC containing diatomite are shown in Fig. 4d. The number of cracks formed in D0, D1, D3, and D5 specimens was 47, 38, 29, and 32, which corresponds to the above statement that the increase in fracture toughness of HS-ECC matrix reduced the probability of the generation of cracks. Furthermore, the average crack width of D0, D1, D3, and D5 specimens were 66, 68, 80, and 74 μm, respectively. With increasing the diatomite content, the crack widths in HS-ECC first increased and then decreased. Incorporating a small amount of diatomite tends to increase the crack width of HS-ECC because that fewer cracks occur in the crack elongation area. The increase in crack width raises the risk of ingress of harmful ions and decreases the self-healing ability of ECC [9, 37]. Additionally, a representative crack pattern of HS-ECC with various diatomite contents is observed in Fig. S6. Although crack number of HS-ECC with diatomite was lower than that in the control specimen (D0), all HS-ECC mixtures showed the obvious multiple narrow cracks.

3.4 Autogenous shrinkage

The influence of diatomite content on the autogenous shrinkage of HS-ECC is shown in Fig. 5a. The 14-d autogenous shrinkage values of D1, D3, and D5

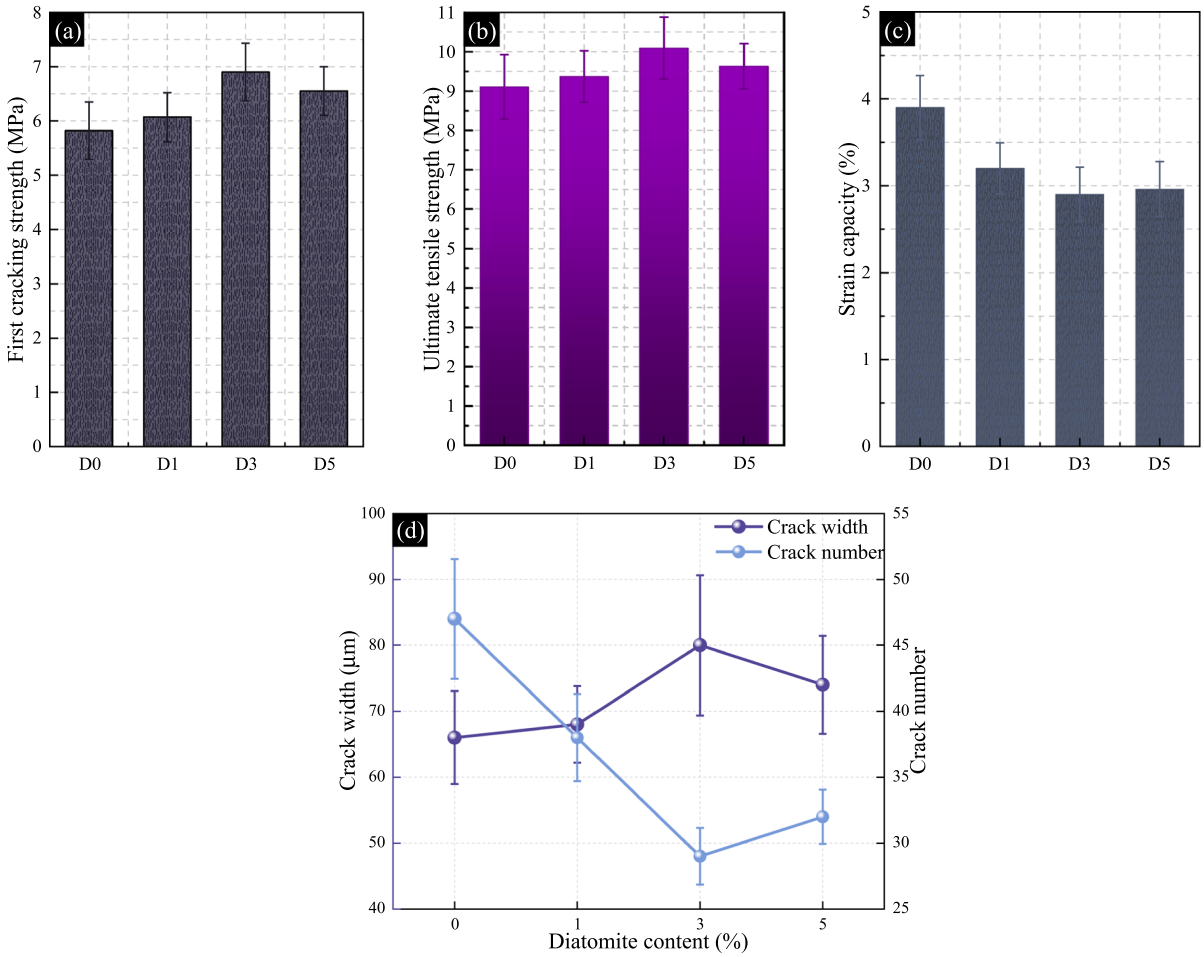

Fig. 4 Tensile parameters of HS-ECC with various diatomite contents. (**a**) First cracking strength, (**b**) Ultimate tensile strength, (**c**) Strain capacity, and (**d**) Crack width and number

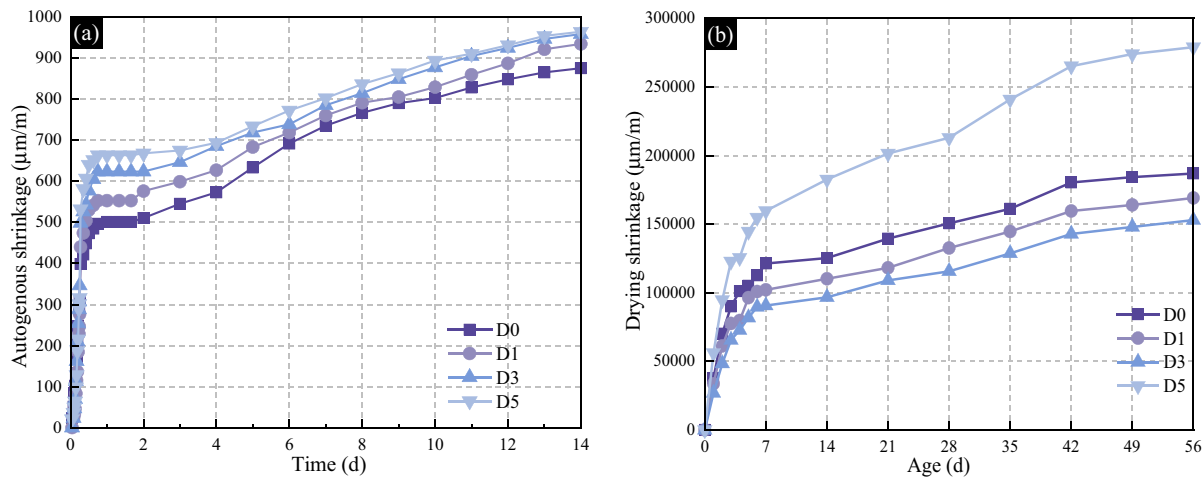

Fig. 5 The shrinkage deformation of HS-ECC containing diatomite. (**a**) Autogenous shrinkage and (**b**) Drying shrinkage

specimens were 935, 959, and 964 μm/m, which is 6.9%, 9.6%, and 10.2% higher than that of D0 specimen, respectively. Therefore, the incorporation of diatomite leads to increasing autogenous shrinkage of HS-ECC. With the increase of diatomite replacement ratio, the autogenous shrinkage of HS-ECC increased. In general, autogenous shrinkage in cement-based materials is related to the pressure in capillary pores, which is mainly determined by the surface tension and the internal humidity of the specimen [38]. As a pozzolanic material, the incorporation of diatomite can improve the hydration degree, which reduces the internal humidity of the matrix. Therefore, the capillary pressure of HS-ECC gradually increases with the increase of the diatomite replacement ratio, and the autogenous shrinkage gradually increases. In addition, the porous diatomite particle absorbs water, resulting in reducing the effective water/binder ratio. This also caused the increase of autogenous shrinkage of HS-ECC paste. Compared with the improvement of hydration degree and the reduction of effective water/binder ratio, the internal curing effect of diatomite may be insufficient to mitigate the autogenous shrinkage. Additionally, the finer diatomite has a higher specific surface area, which also exacerbates autogenous shrinkage. Although D5 paste exhibited the highest 14-day autogenous shrinkage, it was only 10.2% higher than that of the D0 paste.

3.5 Drying shrinkage

The development of drying shrinkage of HS-ECC with different diatomite contents is shown in Fig. 5b. Compared with the D0 sample, the 56-day drying shrinkage of the D1 and D3 samples was lower by 9.5 and 18.2%, respectively. With increasing the diatomite content, the drying shrinkage of HS-ECC gradually reduced. Incorporating diatomite improves the hydration degree of cementitious materials and then increases the compactness of HS-ECC, which finally reduces the path of water evaporation in the specimen. Meanwhile, the filling effect of diatomite also increases the compactness of the specimen, thereby delaying the loss of water. Further, the stiffness of the samples increases with increasing diatomite content, which is also beneficial to improve the volume stability of the specimen. In addition, internal curing effect of diatomite also reduces the drying shrinkage of the ECC. Therefore, the drying shrinkage of the D1 and D3 samples were lower than that of the D0 sample. When the diatomite content exceeded 3%, the drying shrinkage of D5 was higher than that of the reference specimen (D0). The dilution effect of diatomite maybe significantly decrease the hydration degree of paste, making its pore structure coarser, thereby accelerating the loss of moisture from the matrix [39].

3.6 Microstructural analyses

3.6.1 XRD

The XRD results of HS-ECC paste with different diatomite contents are shown in Fig. 6. The types of diffraction peaks of D0, D1, D3, and D5 pastes were the same, including AFt, CH, SiO_2, C_2S, C_3S, and $CaCO_3$. The peak intensity of CH of D1 was higher than that of the reference sample (D0), which may be due to the internal curing effect of diatomite. During the curing process, diatomite releases internal curing water to promote hydration, thereby increasing the CH content. As the replacement ratio of diatomite further increased, the peak intensity of CH of HS-ECC gradually decreased. During the curing process, diatomite has the pozzolanic reaction increasing the amount of hydration products of HS-ECC by the consumption of CH. Furthermore, the incorporation of diatomite reduces the cement content, which also reduces CH content. The pozzolanic reaction and dilution effect of diatomite significantly reduced the

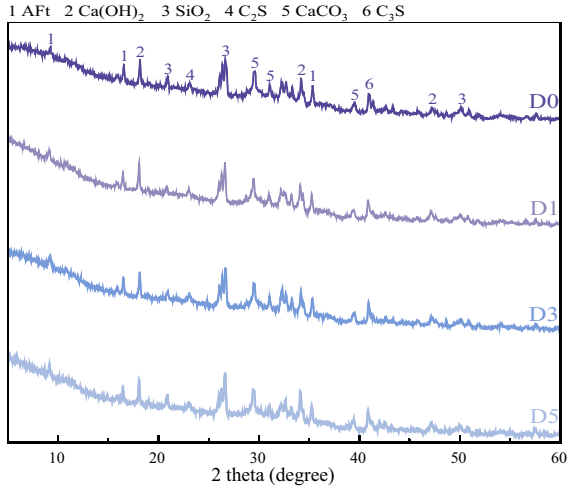

Fig. 6 XRD pattern of HS-ECC with various diatomite contents

CH content when the diatomite content exceeded 1%. Moreover, the peak of $CaCO_3$ is found in all pastes, and it probably is due to the carbonation of CH during the sample preparation process. The incorporation of diatomite significantly increased the SiO_2 content. Incorporating diatomite also resulted in a reduction in the unhydrated phase (C_2S and C_3S) content, which is related to the reduction in cement content and the internal curing effect of diatomite.

3.6.2 DTG

Four groups of samples at 28 days are subjected to the DTG test, including D0, D1, D3, and D5 samples (See Fig. 7a). In general, the peak at 80–130 °C is caused by the decomposition of AFt and C–S–H gels. The peak near 130–230 °C is caused by the dehydration of AFm. The peak at 410–500 °C occurs due to the decomposition of CH [40]. The peak at 500−780 °C mainly originates from the decomposition of $CaCO_3$. Moreover, the formation of $CaCO_3$ is due to the carbonization of CH during the sample preparation process.

The CH content in HS-ECC paste with different diatomite contents was evaluated, as shown in Fig. 7b. With the increase in diatomite content, the trend of CH content is the same as the results of the XRD test. The D1 sample exhibited an increase in CH content compared to the reference HS-ECC (D0), which is due to the internal curing of diatomite. However, the CH content was reduced when the diatomite content exceeded 1%, which is primarily caused by the pozzolanic reactivity of diatomite. This may also be related to the dilution effect of diatomite, which reduces the hydration degree of paste. The change in NEWC can reflect the reaction degree of cementitious material. Incorporating a small amount of diatomite promoted the reaction of cementitious material due to the internal curing pozzolanic effects, which corresponds with the improvement of mechanical properties of HS-ECC. When the diatomite content exceeded 1%, the NEWC of HS-ECC gradually reduced, which may be mainly due to the reduction of cement content.

3.6.3 FT-IR

The FT-IR spectrum of HS-ECC with various diatomite contents at 28 days is shown in Fig. 8. The main characteristic absorption peaks and corresponding group vibrations of HS-ECC with diatomite are as follows. The 3645 cm^{-1} corresponds to the O–H stretching vibration peak of CH [40], and the OH of water vibrates at 1681 cm^{-1} [41]. The 871, 1421, and 2357 cm^{-1} correspond to the C–O stretching vibration peak of carbonate [42, 43]. The 1118 cm^{-1} corresponds to the S–O stretching vibration peak of ettringite [44], and 970 cm^{-1} corresponds to the Si–O stretching vibration peak of the C–S–H gel.

The FT-IR patterns of HS-ECC paste with different diatomite contents are very similar. The characteristic absorption peak of the paste changes in the FT-IR spectrum with the incorporation of diatomite,

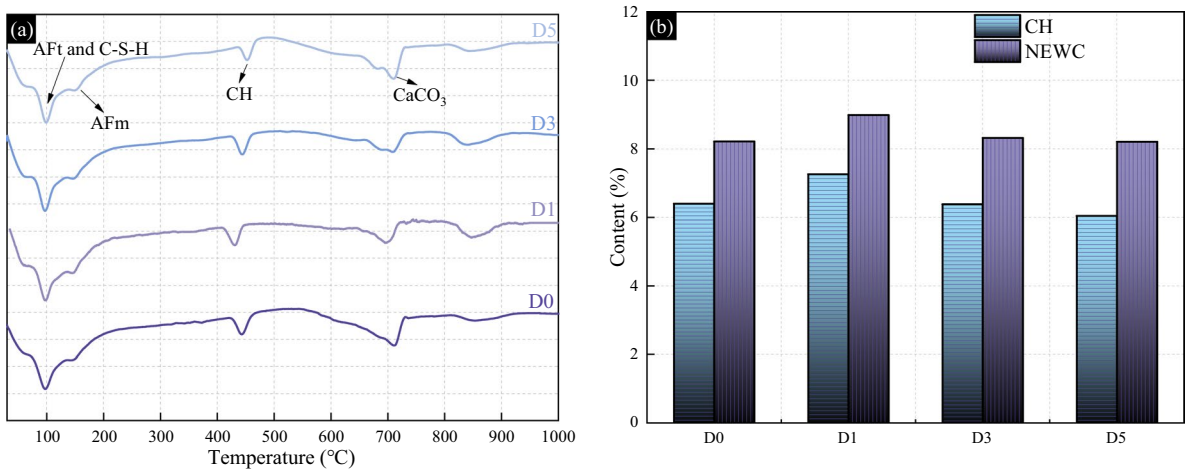

Fig. 7 The DTG result of HS-ECC paste with various diatomite contents at 28 d, (**a**) DTG curves and (**b**) NEWC and CH content

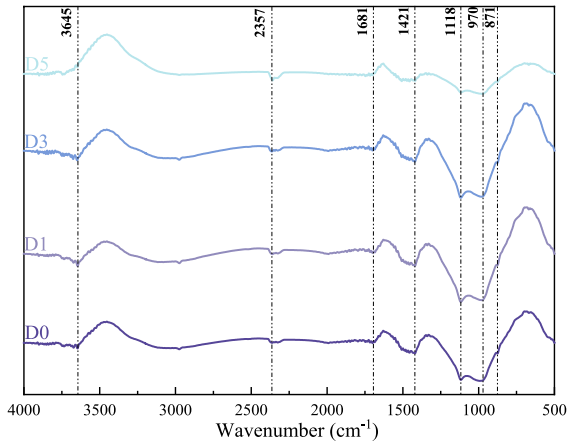

Fig. 8 FT-IR spectrum of 28-d HS-ECC paste with various diatomite contents

which indicates that diatomite influences the hydration process of the binder. With the increase in diatomite content, the intensity of the absorption peak at 3645 cm^{-1} first increases and then decreases. Among all groups, the intensity of the absorption peak at 3645 cm^{-1} of D1 reached the highest value. This is consistent with the results of XRD and DTG analyses, indicating that the internal curing effect of diatomite significantly improves the hydration degree and generates more CH when the diatomite content is 1%. When the diatomite exceeded 1%, combining the pozzolanic reaction and dilution effect of diatomite significantly decreased the CH content of the mixture. The area of the transmission band from 500 to 1500 cm^{-1} also first increased and then decreased with increasing diatomite content, which indicates that different amorphous phases were formed. Unfortunately, this could only be analyzed qualitatively since the device was not able to detect infrared absorption in the low wavenumber range.

3.6.4 MIP

Pores can be classified into more-harmful pores (> 200 nm), harmful pores (50−200 nm), less-harmful pores (20−50 nm), and harmless pores (< 20 nm) [45]. The cumulative pore curves and pore size distribution of HS-ECC paste containing diatomite at 28 days are shown in Fig. 9a and b, respectively. Compared with D0, the porosity of D1, D3, and D5 specimens decreased by 1.6, 18.32, and 9.72%, respectively. The porosity of HS-ECC paste first decreased and then increased with the increase of diatomite content. When the content of diatomite was 3%, the porosity of HS-ECC was the lowest.

Incorporating diatomite refines the pore structure of the samples, as presented in Fig. 9b. When the diatomite content increased from 0 to 3%, the more-harmful pores, harmful pores, and less-harmful pores of the sample gradually decreased. Meanwhile, the more-harmful porosity of the D5 sample was only 32% of control sample. This implies that the use of

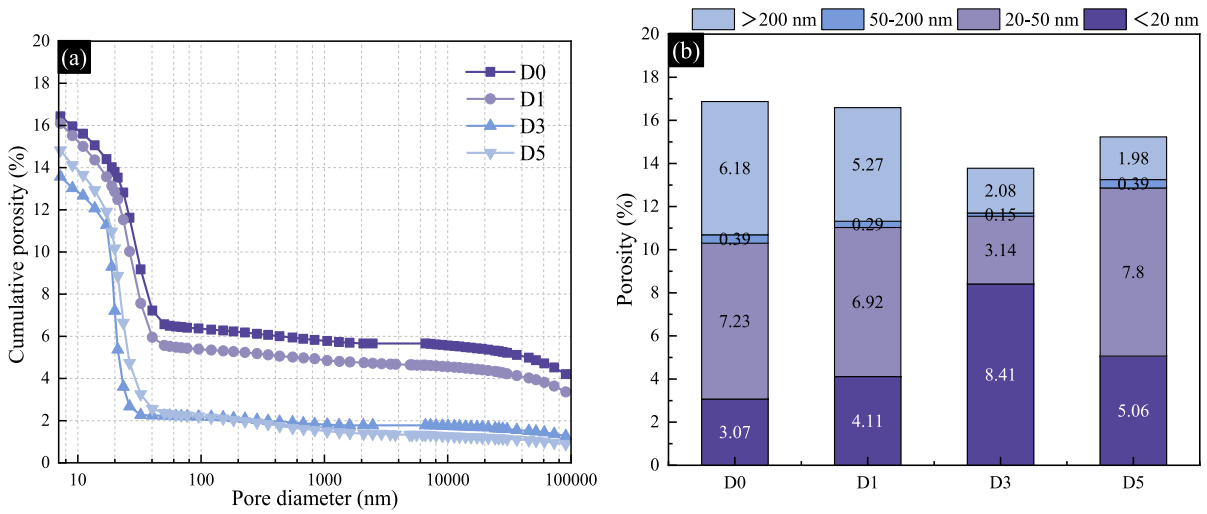

Fig. 9 Pore structure of HS-ECC with various diatomite contents. (**a**) Cumulative porosity curves and (**b**) Pore size distribution

diatomite significantly improves the compactness of the ECC due to the pozzolanic activity and filling effect of diatomite. Additionally, diatomite particles can play an internal curing role, thereby increasing the content of hydration products and improving the pore structure of the samples. However, it was also found that the porosity of D5 was higher than that of D3, indicating that incorporating excessive diatomite content decreases compactness of paste due to the dilution effect of diatomite.

3.6.5 SEM

The morphology of the fiber in the HS-ECC with different diatomite contents after the tensile experiment is shown in Fig. 10. There were different damage degrees of fiber in the HS-ECC matrices with different diatomite contents. The damage gradually increased with the increase of diatomite content up to 3%. When the diatomite content was 3%, the damage degree of fiber was the most serious. This is because the incorporation of 3% diatomite greatly improved the compactness of the matrix, thereby enhancing the cohesion force of the fiber/matrix interface. Compared with the D0, the slip of fibers in D1 and D3 samples require more tensile loading, and their damage is more serious. Moreover, the damage degree of fiber of the D5 sample is slightly weaker than that of the D3 sample, which is attributed to the dilution effect of diatomite.

4 Environmental impact and economic benefits

Table 3 shows the economic and environmental benefits per cubic meter of ECC mixtures without fiber. Generally, parameters such as GWP, nr-CED, ODP, NP, and POCP of ECC mixtures decreased with increasing diatomite content. However, the incorporation of a small amount of diatomite also increased the cost and AP value of the ECC mixture, which is mainly due to the increase in SP content caused by the incorporation of diatomite. With the further increase of diatomite content, the economic and environmental benefits of ECC mixtures were significantly reduced, which is mainly contributed by the low environmental and economic burden of diatomite.

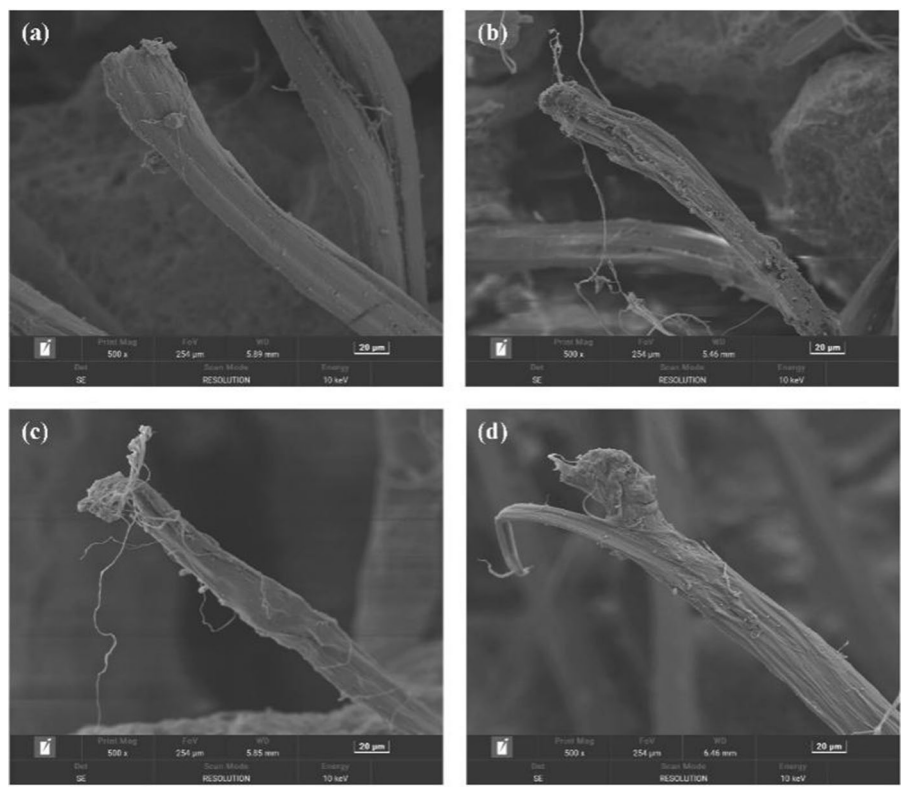

Fig. 10 Morphology of fiber after the tensile experiment. (**a**) D0, (**b**) D1, (**c**) D3, and (**d**) D5

Table 3 The economic and environmental benefits per cubic meter of ECC mixtures without fiber

Mixture	GWP (kg CO_2-eq)	nr-CED (MJ)	ODP (kg CFC11-eq)	NP (kg PO_4-eq)	AP (kg SO_2-eq)	POCP (kg C_2H_4-eq)	Cost (USD)
D0	537.45	2333.96	1.37×10^{-5}	0.194	0.761	0.202	246.03
D1	533.00	2333.88	1.37×10^{-5}	0.193	0.763	0.202	246.23
D3	523.33	2319.15	1.36×10^{-5}	0.192	0.758	0.201	245.69
D5	514.02	2311.43	1.35×10^{-5}	0.191	0.758	0.201	245.60

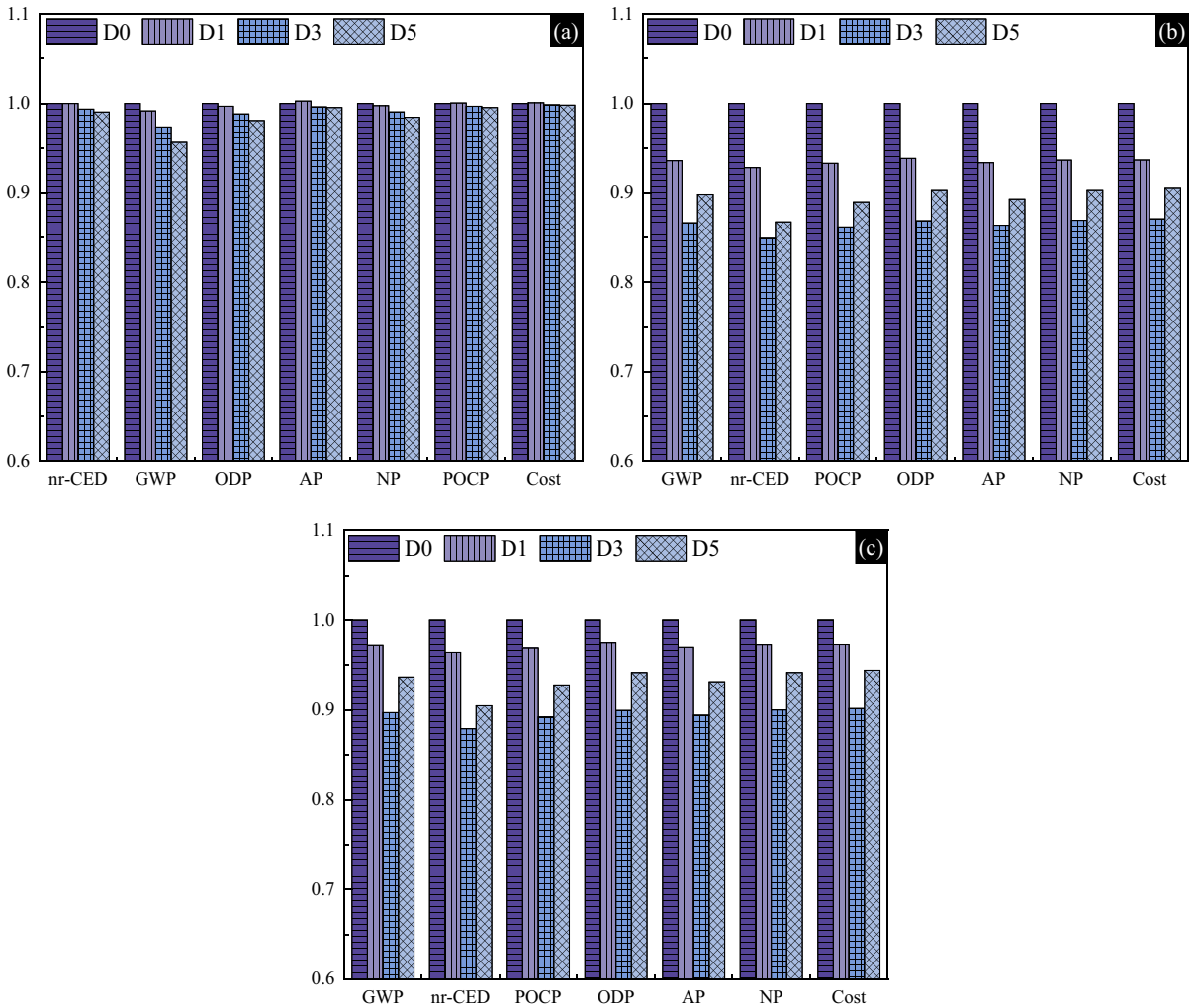

Fig. 11 Normalized economic and environmental benefits of ECC without fiber. (**a**) per cubic meter of ECC, (**b**) per cubic meter of ECC per MPa of compressive strength, and (**c**) per cubic meter of ECC per MPa of tensile strength

The normalized environmental and economic benefits of the ECC mixture is shown in Fig. 11. Considering that these mixtures have different mechanical properties, the ratios of these indices to strength (28-d compressive strength and tensile strength) were adopted, as shown in Fig. 11b–c. With increasing the diatomite content, the cost and environmental parameters of the ECC mixture per unit strength were

significantly decreased. When the diatomite content reached 3%, the unit strength cost and environmental burden per cubic meter of ECC mixture reached the lowest level. In terms of cost and environmental benefit per unit compressive strength mixture, cost, nr-CED, GWP, ODP, AP, NP, and POCP of the D3 mixture were reduced by 12.9, 15.1, 13.3, 13.1, 13.6, 13.1, and 13.8%, respectively, relative to the reference ECC mixture.

Figure 12 is a radar chart of the economic and environmental benefits of diatomite-modified ECC mixtures. The incorporation of diatomite was the most significance for reducing the GWP of the ECC mixture (Fig. 12a). Due to the low substitution level of diatomite, the cost of diatomite-modified ECC was similar to that of plain ECC. For the economic and environmental benefits of the mixture per unit strength (Fig. 12b), the effect of adding diatomite was significant because it effectively improved the mechanical properties of ECC. The D3 mixture had the lowest cost and environmental benefits per unit strength, and it showed the most significant reduction in nr-CED.

5 Discussion

5.1 Influence of diatomite on the ECC properties

The influence mechanism of diatomite on cementitious composites is shown in Fig. 13. The influence is mainly divided into three aspects. Due to its small particle size (see Fig. S1), diatomite fills the internal pore of sample, thereby reducing porosity and improving the pore structure of the ECC specimen. Compared to the reference ECC samples, the macropore (size > 50 nm) content of the diatomite samples was significantly reduced, i.e., the pore structure of the ECC matrix was refined by the incorporation of diatomite (see Fig. 9). In general, pore structure refinement is very beneficial for compressive strength development of cement-based materials. Furthemore, diatomite is mainly composed of SiO_2, and its SiO_2 content is higher than 93% (see Table 1). In the hydrating cement, the amorphous SiO_2 consumes CH and produces C–S–H gel, which was confirmed by the results of DTG. The increase in C–S–H gel content promoted the compressive strength development of HS-ECC. Additionally, diatomite has a porous structure, and its water absorption is as high as 1 g/g. When the internal humidity of the ECC sample decreases due to the hydration of cement, the diatomite particle slowly releases the internal curing water to inhibit the decrease in the pressure of the capillary pore, thereby reducing shrinkage deformation of HS-ECC (see Fig. 5). Meanwhile, the internal curing effect of diatomite also increases the hydration degree of HS-ECC paste and its reaction degree (see Fig. 7).

As mentioned above, diatomite displays an excellent filling effect, pozzolanic activity, and internal curing effect in the cement system. Incorporating

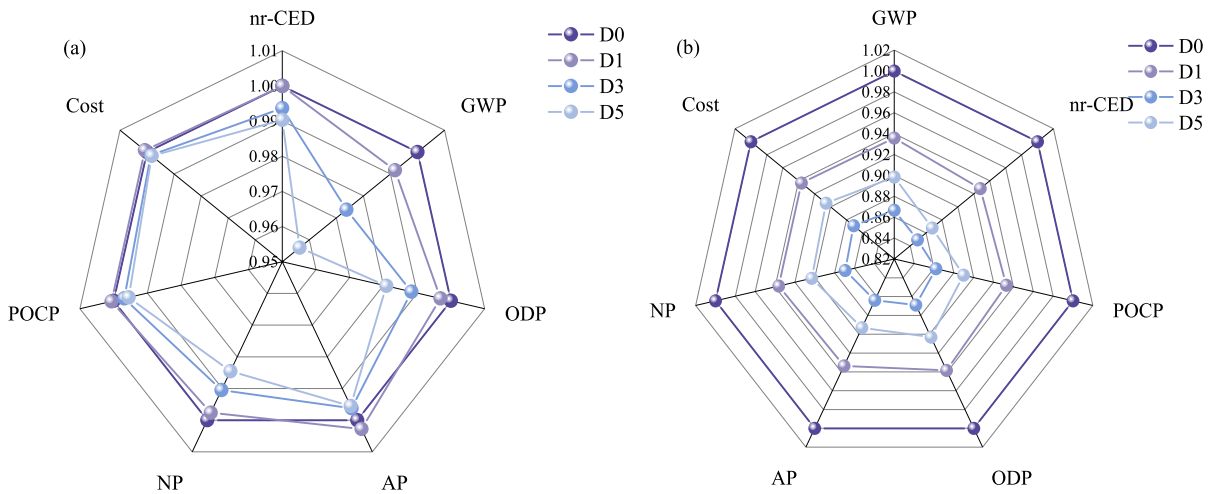

Fig. 12 The normalized economic and environmental benefits for per cubic meter of ECC mixtures without fiber: (**a**) for per cubic meter of ECC, and (**b**) for per cubic meter of ECC per MPa of compressive strength

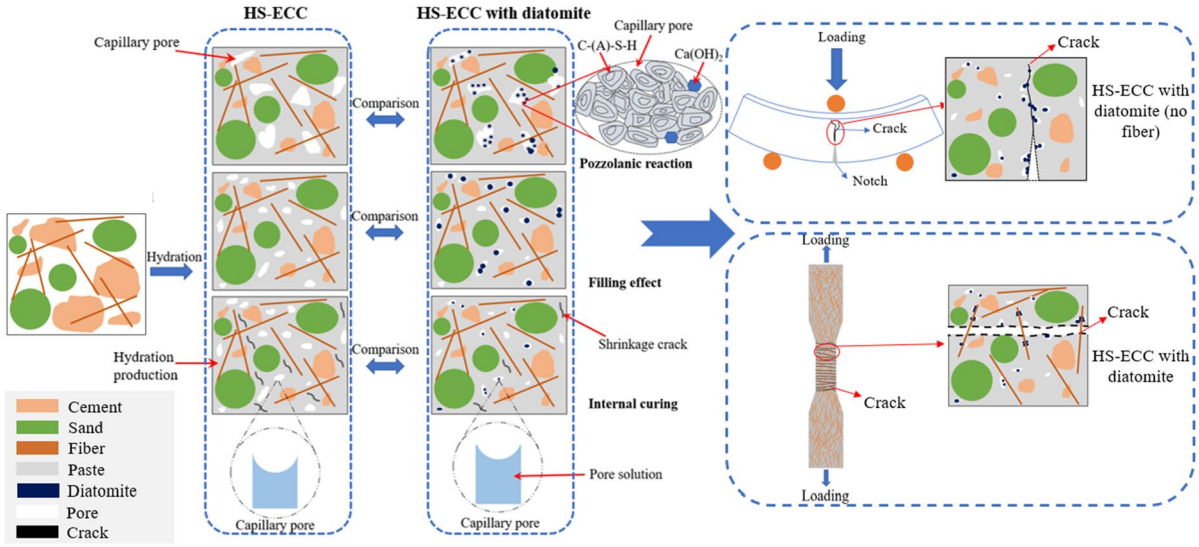

Fig. 13 The postulated mechanism of the effect of diatomite on HS-ECC

diatomite therefore improves the pore structure of the ECC matrix (Fig. 13), and crack initiation requires more energy during the three-point bending test. Therefore, the incorporation of diatomite increases the fracture toughness of the ECC matrix. Moreover, after incorporating diatomite, the compactness of the fiber/matrix interface was improved, resulting in increasing the frictional bonding stress of the fiber/matrix interface in the ECC specimen during the tensile test. Since PE fiber is hydrophobic, the increase in the tensile strength of ECC mainly depends on the frictional bonding stress between the PE fiber and matrix during the tensile test [46]. When this frictional bonding stress is high in ECC, the slip of PE fiber is difficult. The incorporation of diatomite increased the frictional bonding stress of the fiber/matrix interface, so the tensile strength of the ECC gradually enhanced.

5.2 Comparison of diatomite based and other "green" HS-ECCs

The influences of SCMs on the mechanical properties of HS-ECC are summarized in Fig. 14. Among all SCM-modified HS-ECC, diatomite showed the most significant improvement in the compressive strength of HS-ECC. This can be attributed to the low diatomite content and its high reactivity. In terms of strain capacity, the HS-ECC with zeolite powder and

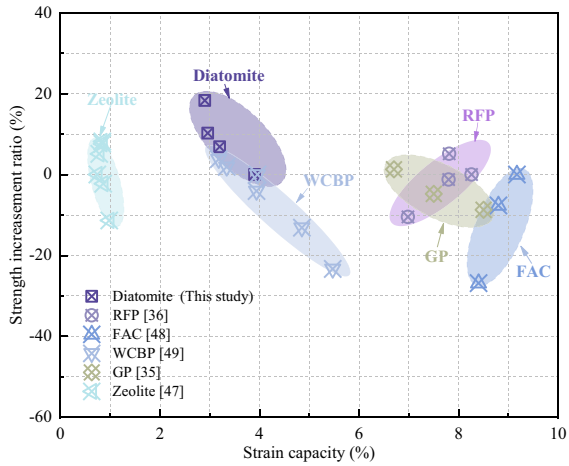

Fig. 14 The influence of SCMs on the strength gain of HS-ECC. Where, strength: the 28-d compressive strength of HS-ECC (28-d compressive strength > 80 MPa), *RFP* recycled fine powder, *GP* glass powder, *FAC* fly ash cenosphere, and *WCBP* waste clay brick powder [35, 36, 47–49]

polyvinyl alcohol (PVA) fiber had the lowest strain capacity with 0.74−0.98% in all samples [47]. The high-strength HS-ECC generally has a high compactness, which indicates that there is a high adhesion force between the fiber/matrix interface. Therefore, PVA fibers are prone to either directly breaking or just having minor slippage under tensile conditions. In other HS-ECCs in Fig. 14, PE fibers were used,

and these samples all have a significant strain capacity. Compared to PVA fiber, PE fiber has a higher tensile strength and elastic modulus, making it easier to achieve strain-hardening behavior. Therefore, the use of PE fibers is a good choice for HS-ECCs. Furthermore, Fig. 14 is also shown that the strain capacity of HS-ECC containing diatomite is worse than that of recycled fine powder, glass powder, and FA cenosphere [35, 36, 48]. This may be due to the high content of GGBS and SF in other HS-ECCs. Not only do GGBS and SF exert the pozzolanic reactivity and filling effect to efficiently improve the fiber bridging capacity, but also significantly improve the fiber dispersion in HS-ECC. Generally, a great fiber dispersion contributes to achieve the excellent strain-hardening behavior of HS-ECC. Although these HS-ECCs with high contents of GGBS and SF have the excellent strain-hardening performance in literature [35, 36, 47, 49], the incorporation of GGBS and SF also increase the cost of HS-ECCs with recycled fine powder, glass powder, and FA cenosphere.

The cost and GWP of raw materials in different HS-ECC mixtures are listed in Table S2. After calculation, the total cost and GWP of HS-ECC specimen per cubic meter are presented in Fig. 15. The total cost of HS-ECC containing diatomite is the lowest among all HS-ECCs, which is due to the application of high-volume FA. This has great significance to the sustainability of HS-ECC. Besides, the GWP of HS-ECC with diatomite is 525.1−538.3 kg/m^3, which is lower than that of HS-ECC with WCBP and GP due to its low cement content (See Fig. 15b). Due to its lower substitution level, the impact of diatomite replacement on the carbon footprint reduction among is relatively low. Li et al. [19] found that the 28-day compressive strength of mortar did not decrease when the 30−40% diatomite was incorporated. Meanwhile, Ahmadi et al. [32] found that the incorporation of 30% diatomite increased by 28.4% of the tensile strength of mortar. This implies that the high-volume diatomite may also be beneficial for improving the tensile strength of HS-ECC. Therefore, the high-volume diatomite can further be used to improve economic and environmental benefits of HS-ECC.

6 Conclusions

This study aims to develop eco-friendly high-strength engineered cementitious composites (HS-ECC) and investigate their mechanical behavior, volume deformation, microstructure, economic, and environmental benefits. In areas rich in diatomite, this allows to reduce the environmental load and improve the strength of HS-ECC. Based on these results, the following conclusions can be drawn:

(1) The incorporation of a small amount of diatomite can effectively increase the strength of HS-ECC, making the 28-day compressive strength of the sample reach 101.7 MPa. At the composite level, the tensile strength and the first cracking

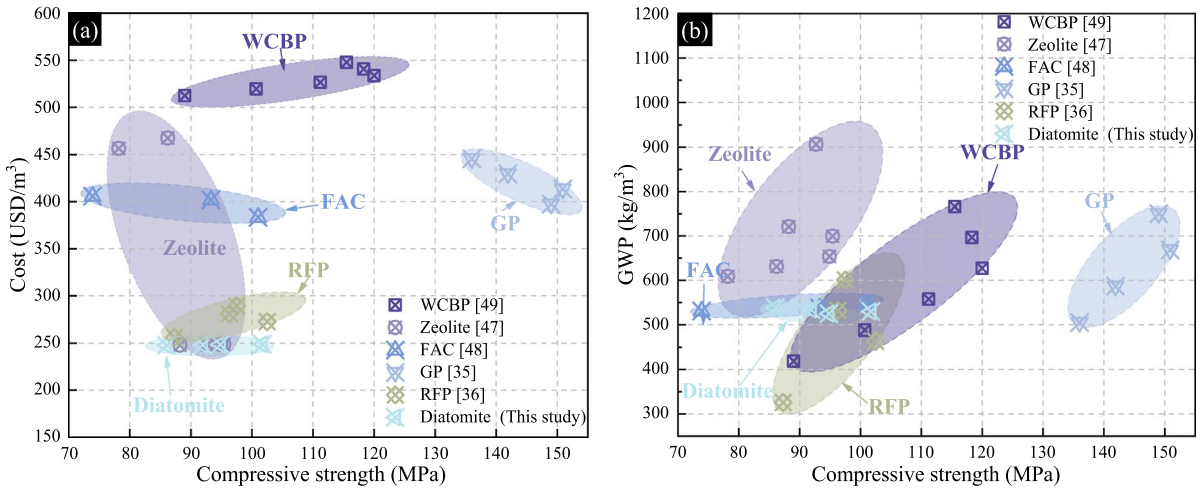

Fig. 15 Cost and GWP of HS-ECC with different types of SCMs (without fiber), (**a**) Cost, and (**b**) GWP [35, 36, 47–49]

strength of HS-ECC increased with the substitution of cement by diatomite, of which the specimen mixed with 3% diatomite showed the highest value.

(2) Due to its high specific surface area and pozzolanic activity, the incorporation of diatomite increased the autogenous shrinkage of the HS-ECC mixture, but the increase was limited (up to 10%). On the other hand, incorporating an appropriate amount of diatomite can reduce the drying shrinkage of HS-ECC due to its internal curing effect and its improvement on the pore structure.

(3) In the HS-ECC mixture, diatomite has a filling effect, an internal curing effect, and pozzolanic activity, which increases the hydration degree of mixture. This possibly further improves the matrix compactness and the bonding of fiber/matrix interface, which increases the strength of the composite.

(4) The incorporation of diatomite reduced the porosity of the 28-day sample and refined its pore structure. Among the samples, HS-ECC with 3% diatomite had the smallest porosity, which increased the difficulty of fiber slippage. This was consistent with the most serious damage of fiber at the HS-ECC with 3% diatomite. Furthermore, the HS-ECC with 3% diatomite had the lowest number of cracks and the largest crack width.

(5) HS-ECC with diatomite performed exceptionally well on non-renewable cumulative energy demand (nr-CED) and global warming potential (GWP). For the per cubic meter of HS-ECC per MPa of compressive strength, the cost, nr-CED, and GWP of the sample mixed with 3% diatomite were reduced by 12.9, 15.1, and 13.3%, respectively, relative to the plain mixture.

A novel HS-ECC was successfully prepared using diatomite in this study, and the multiple roles of diatomite in ECC were systematically investigated and explained through mechanical behavior development, microstructural characterization and environmental assessment, which provides a reference for the application of diatomite in traditional cement-based materials (fiber-reinforced concrete and concrete with low water-binder ratio). Meanwhile, single-cracking and single fiber pull-out tests will be considered in future research, because it is beneficial to understand the influence mechanism of diatomite on ECC fiber/matrix interface, fiber bridging force and mechanical behaviors from the perspective of multi-scale effects.

Funding None.

Declarations

Competing interest None.

References

1. Wu Z, Khayat KH, Shi C et al (2021) Mechanisms underlying the strength enhancement of UHPC modified with nano-SiO_2 and nano-$CaCO_3$. Cement Concrete Comp 119:103992
2. Jiang J, Feng T, Chu H et al (2019) Quasi-static and dynamic mechanical properties of eco-friendly ultra-high-performance concrete containing aeolian sand. Cem Concr Comp 97:369–378
3. Van Mier JGM (1996) Fracture processes of concrete. CRC Press
4. Savija B (2014) Experimental and numerical investigation of chloride ingress in cracked concrete. Delft University of Technology, Delft, Netherlands
5. Blagojevic A (2016) The influence of cracks on the durability and service life of reinforced concrete structures in relation to chloride-induced corrosion. Technical University of Delft, Delft, Netherlands
6. Liu D, Yu J, Qin F et al (2023) Mechanical performance of high-strength engineering cementitious composites (ECC) with hybriding PE and steel fibers. Case Stud Constr Mater 18:e01961
7. Ding Y, Yu K, Li M (2022) A review on high-strength engineered cementitious composites (HS-ECC): design, mechanical property and structural application. Structures 35:903–921
8. Wang L, Rehman NU, Curosu I et al (2021) On the use of limestone calcined clay cement (LC3) in high-strength strain-hardening cement-based composites (HS-SHCC). Cem Concr Res 144:106421
9. Wang L, Zhu Z, Ahmed AH et al (2023) Self-healing behavior of high-strength strain-hardening cement-based composites (HS-SHCC) blended with limestone calcined clay cement (LC3). Constr Build Mater 370:130633
10. Sun C, Ge W, Zhang Y et al (2023) Designing low-carbon cement-free binders for stabilization/solidification of MSWI fly ash. J Environ Manage 339:117938
11. Huang BT, Weng KF, Zhu JX et al (2021) Engineered/strain-hardening cementitious composites (ECC/SHCC) with an ultra-high compressive strength over 210 MPa. Compos Commun 26:100775
12. Yao Y, Zhu Y, Yang Y (2012) Incorporation superabsorbent polymer (SAP) particles as controlling pre-existing flaws to improve the performance of engineered cementitious composites (ECC). Constr Build Mater 28(1):139–145

13. Wu H, Yu J, Du Y et al (2021) Mechanical performance of MgO-doped engineered cementitious composites (ECC). Cem Concr Comp 115:103857
14. Zhang Z, Liu S, Yang F et al (2021) Sustainable high strength, high ductility engineered cementitious composites (ECC) with substitution of cement by rice husk ash. J Clean Prod 317:128379
15. Xiao LG, Zhao Z, Yu WZ (2010) Development status and Prospect of diatomite at home and abroad. J Jilin Jianzhu Univ 27:26–30 ((**In Chinese**))
16. Tsai WT, Hsien KJ, Lai CW (2004) Chemical activation of spent diatomaceous earth by alkaline etching in the preparation of mesoporous adsorbents. Ind Eng Chem Res 43(23):7513–7520
17. Lemons JF (1997) Diatomite. Am Ceram Soc Bull 76(6):92–95
18. Wang L, Zhang Y, Chen L et al (2022) Designing novel magnesium oxysulfate cement for stabilization/solidification of municipal solid waste incineration fly ash. J Haz Mat 423:127025
19. Li J, Zhang W, Li C et al (2020) Eco-friendly mortar with high-volume diatomite and fly ash: performance and life-cycle assessment with regional variability. J Clean Prod 261:121224
20. Li J, Zhang W, Li C et al (2019) Green concrete containing diatomaceous earth and limestone: workability, mechanical properties, and life-cycle assessment. J Clean Prod 223:662–679
21. Degirmenci N, Yilmaz A (2009) Use of diatomite as partial replacement for Portland cement in cement mortars. Constr Build Mater 23(1):284–288
22. Jud Sierra E, Miller SA, Sakulich AR et al (2010) Pozzolanic activity of diatomaceous earth. J Am Ceram Soc 93(10):3406–3410
23. Crangle Jr RD (2018) Diatomite: advanced release. In: 2016 Minerals Yearbook. US Geological Survey & US Department of the Interior, Washington, pp 22.1–22.5
24. Zhang M, Zhu X, Pyo S et al (2023) Feasibility of using high-volume pozzolanic fillers to develop sustainable engineered cementitious composites (ECC). Powder Technol 428:118853
25. Chinese National Standard (1999) Method of testing cements–Determination of strength. (GB/T 17671-1999). Beijing. (In Chinese)
26. American Society for Testing and Materials (1994) Test Method for Plane-Strain Fracture Toughness of Metallic Materials (ASTM E399–90), Philadelphia
27. Xu S, Reinhardt HW (1999) Determination of double-K criterion for crack propagation in quasi-brittle fracture, Part II: analytical evaluating and practical measuring methods for three-point bending notched beams. Int J Fract 98(2):151–177
28. Committee JC (2008) Recommendations for design and construction of high performance fiber reinforced cement composites with multiple fine cracks. Japan Society of Civil Engineers, Tokyo, Japan
29. American Society for Testing and Materials (2001) Standard test method for drying shrinkage of mortar containing hydraulic cement (ASTM C596-01). Philadelphia
30. Chen W, Hong J, Xu C (2015) Pollutants generated by cement production in China, their impacts, and the potential for environmental improvement. J Clean Prod 103:61–69
31. Ahmadi Z, Esmaeili J, Kasaei J et al (2018) Properties of sustainable cement mortars containing high volume of raw diatomite. Sustain Mater Techno 16:47–53
32. Sarıdemir M, Çelikten S, Yıldırım A (2020) Mechanical and microstructural properties of calcined diatomite powder modified high strength mortars at ambient and high temperatures. Adv Powder Technol 31(7):3004–3017
33. Kastis D, Kakali G, Tsivilis S et al (2006) Properties and hydration of blended cements with calcareous diatomite. Cem Concr Res 36(10):1821–1826
34. Zhou Y, Gong G, Huang Y et al (2021) Feasibility of incorporating recycled fine aggregate in high performance green lightweight engineered cementitious composites. J Clean Prod 280:124445
35. Wu JD, Guo LP, Cao YZ et al (2022) Mechanical and fiber/matrix interfacial behavior of ultra-high-strength and high-ductility cementitious composites incorporating waste glass powder. Cem Concr Comp 126:104371
36. Yu KQ, Zhu WJ, Ding Y et al (2019) Micro-structural and mechanical properties of ultra-high performance engineered cementitious composites (UHP-ECC) incorporation of recycled fine powder (RFP). Cem Concr Res 124:105813
37. Šavija B, Schlangen E, Pacheco J et al (2014) Chloride ingress in cracked concrete: a laser induced breakdown spectroscopy (LIBS) study. J Adv Concr Technol 12(10):425–442
38. Kang J, Shen D, Li C et al (2022) Effect of water-to-cement ratio on internal relative humidity and autogenous shrinkage of early-age concrete internally cured by super-absorbent polymers. Struct Concr 23(5):3234–3248
39. Yalçinkaya Ç, Felekoğlu B, Yazici H (2020) Agrega hacminin ultra yüksek performanslı betonun büzülme, reolojik ve mekanik özelliklerine etkisi. Gazi Üniversitesi Mühendislik Mimarlık Fakültesi Dergisi 35(4):1701–1718
40. Kocak Y, Nas S (2014) The effect of using fly ash on the strength and hydration characteristics of blended cements. Constr Build Mater 73:25–32
41. Shukla P, Bhatia V, Gaur V et al (2012) Multiwalled carbon nanotubes reinforced cement composite based room temperature sensor for smoke detection. Sens Transd 146(11):48
42. Preetham HS, Madhu GM, Brijesh B et al (2016) High temperature CO_2 sorption using $Ca(OH)_2$ in pilot scale packed column. Eur J Chem 7(2):176–181
43. Zhou Y, Wang Z, Zhu Z et al (2021) Impacts of space restriction on the microstructure of Calcium Silicate Hydrate. Materials 14(13):3645
44. Biricik H, Sarier N (2014) Comparative study of the characteristics of nano silica-, silica fume-and fly ash-incorporated cement mortars. Mater Res 17:570–582
45. Zhang M, Li H (2011) Pore structure and chloride permeability of concrete containing nano-particles for pavement. Constr Build Mater 25(2):608–616
46. Ma H, Yi C, Wu C (2021) Review and outlook on durability of engineered cementitious composite (ECC). Constr Build Mater 287:122719
47. Xuan Z, Jun Z (2021) Influence of zeolite addition on mechanical performance and shrinkage of high strength

engineered cementitious composites. J Build Eng 36:102124
48. Zhou Y, Xi B, Sui L et al (2019) Development of high strain-hardening lightweight engineered cementitious composites: design and performance. Cem Concr Comp 104:103370
49. Wu JD, Guo LP, Qin YY (2021) Preparation and characterization of ultra-high-strength and ultra-high-ductility cementitious composites incorporating waste clay brick powder. J Clean Prod 312:127813